ROBOMECH Journal

RESEARCH ARTICLE

Open Access

High-strength and flexible mechanism for body weight support

Sojiro Sugiura[1*], Jayant Unde[1], Yaonan Zhu[1] and Yasuhisa Hasegawa[1]

Abstract

Wearable body weight support systems can assist individuals with mobility impairments in performing daily living activities with greater ease and independence. However, existing systems have limitations in terms of balancing their strength, compact size, interaction with the ground, and driving. In this paper, we present the High-Strength and Flexible Mechanism (HSFM) designed for body weight support. The HSFM utilizes a coiling truss mechanism to perform flexible transformation between a straight and spiral shape. Its complex linkages create the mechanical constraints of the structure and enhance its stiffness. Additionally, the HSFM achieved a high extension rate, effective wire-driven mechanism, and smooth shift of the grounding point. We provide a detailed description of the HSFM, including the simplest 4-linkage mechanism, its mechanical constraints, and the wire-driven mechanism. Moreover, we conducted parametric analysis and geometric calculation on the link structure. The results justified the mechanical constraints of the HSFM and ensured the high extension rate. Further, its functionality for body weight support was evaluated with the hardware and showed sufficient results in terms of strength, smooth grounding, and wire-driven. This novel mechanism has the potential to develop a wearable body weight support robot enhancing daily living activities such as sit-to-stand transfer and walking.

Keywords High-strength and flexible mechanism, Body weight support, Wire driven, Parallel link, Mechanical robotics

Introduction

Assistance devices for daily living activities have been developed to assist individuals with disabilities or mobility impairments in performing everyday tasks such as sit-to-stand and walking. Body weight support systems can be particularly useful in these contexts, as they support the individual's body weight during activities that might otherwise be challenging or impossible.

Various devices have been developed to provide body weight support. Robotic caster walkers [1, 2] are capable of supporting the user's body weight and improving the safety and stability of walking movements. However, they tend to be bulky and have limited mobility on stairs. Harness-type systems have a high capacity to prevent falls, but their installation requires large-scale structures, such as ceiling construction [3, 4]. On the other hand, robotic exoskeletons [5–8] are wearable and compact, and they can assist with several movements. However, due to their compact design, their capacity for body weight support is limited. Additionally, these devices do not provide sufficient protection against falls since they are not suspended from the ceiling and yet the support polygon is only the wearer's feet.

Asada et al. have developed limb-type wearable robots that can solve the problem. [9, 10]. They support body weight sufficiently with assistive braces and assist the wearer in maintaining a static posture [11, 12]. The braces expand the support polygon of the wearer and enhance the stability. Additionally, the braces employ linear actuators that offer high force and compactness. However,

*Correspondence:
Sojiro Sugiura
sugiura@robo.mein.nagoya-u.ac.jp
[1] Department of Micro-Nano Systems Engineering, Nagoya University, Aichi, Japan

flexibility, which is the capability of changing posture in response to assistance situations, is limited. Flexibility is important for limb-type wearable robots and body weight support systems, as it provides essential aspects for their functionality.

We focus on two aspects to which flexibility can contribute: extension rate and dynamic grounding. Firstly, flexible mechanisms achieve a high extension rate: they can extend during only assistance, whilst it shrinks at other times. Since they can minimize interference with the user when not assisting, the comfortableness for the wearer will be improved. Secondly, flexibility can enhance the dynamic grounding function. The grounding points of the aforementioned robots are fixed on static points and cannot be applied to assist dynamic activities. However, flexible structures can change their posture based on environmental contact areas and shift their contact points to achieve the assistance for dynamic motions. To increase the variation of assistance such as walking, sit-to-stand, and turning, careful consideration must be given to ground interaction. Therefore, to achieve comfortable and variable body weight support, we need mechanisms that can provide both flexibility and high strength.

Many researchers have aimed to balance robotic arms' strength and flexibility. Deformable arms, for example, can change their postures with many degrees of freedom [13–15]. Origami structures provide high extension rate due to their deplorable mechanism [16, 17]. Additionally, they can get high rigidity to support body weight [18]. Although they have achieved a good balance between their strength and flexibility, their usage for body weight support is limited. This is because they can cause unpredictable deformation under large external forces, which can endanger the wearer such as instability and falling. Another example is parallel linkage mechanisms, which can achieve high strength due to their structural robustness while maintaining a high extension rate [19, 20]. However, they require many actuators to change poses, making the driving system more complex. Conversely, scissor structural mechanisms can be driven with only one actuator, despite being a form of parallel linkage mechanism [21, 22]. However, their strength is ensured by the metallic materials [23] because the mechanism's simplicity cannot provide high structural strength. Since the metallic parts can increase the weight of the mechanism and decrease the comfortableness of the wearer, the strength should be ensured by the mechanism's complexity. In addition, the scissor mechanism still has a limitation regarding the actuators: the longer the scissor mechanism, the more actuating power it requires.

Therefore, by summarizing the above literature, the requirements of the body weight support mechanism for the limb-type robot can be listed as: High structural strength, high extension rate, dynamic interaction with the ground, and simple driving system. The coiling truss mechanism [24] can provide a solution to match those requirements. Coiling truss mechanisms comprise 4 linkage mechanisms and demonstrate a flexible transformation between straight and spiral poses. The high extension rate can be achieved by the unique transformation. Furthermore, the spiral shape will contribute to the continuous shifts on the ground without any slip and fall. The structural strength of this mechanism is expected to be high owing to its singular postures and complex mechanical constraints. However, since the strength of the mechanism is not mentioned in the paper [24], it must be justified with the prototype. Furthermore, the methodology of driving has not yet been developed. The system must transform the pose of the mechanism with as few actuators as possible.

In this paper, we have developed the High-Strength and Flexible Mechanism (HSFM) that satisfies the requirements, as shown in Fig. 1 and Additional file 1 (video format). The mechanism was designed based on the coiling truss mechanism [24]. Its spiral shape makes the interaction of the ground smooth and ensures the high extension rate. The structural strength of the HSFM was investigated on a geometric analysis and was ensured through simulations and real-world experiments. Moreover, the driving system was developed with wires and only one motor. We confirmed that the driving system can transform the shape of the HSFM under external forces.

Contributions that this paper provides are listed below: (1) A mechanism that flexibly transforms between straight and spiral postures while maintaining high structural strength was developed. (2) A wire-driven system for transforming the mechanism was developed by using only one motor. (3) Experiments to evaluate the mechanism in terms of strength, dynamic grounding function, and required wire force were conducted and showed sufficient results for body weight support.

In the following section of this paper, the base mechanism of the HSFM and its 1st prototype are introduced in "Mechanism" Section . Following that, parametric analyses are conducted for understanding the length parameters' effects on the mechanical property in "Parametric analysis" Section. Based on the analysis and tests with the 1st prototype, the 2nd prototype is redesigned and experiments using it are done in "Experiments and discussion" Section. Finally, we discuss the limitations of this study and future plan in "Conclusion" Section.

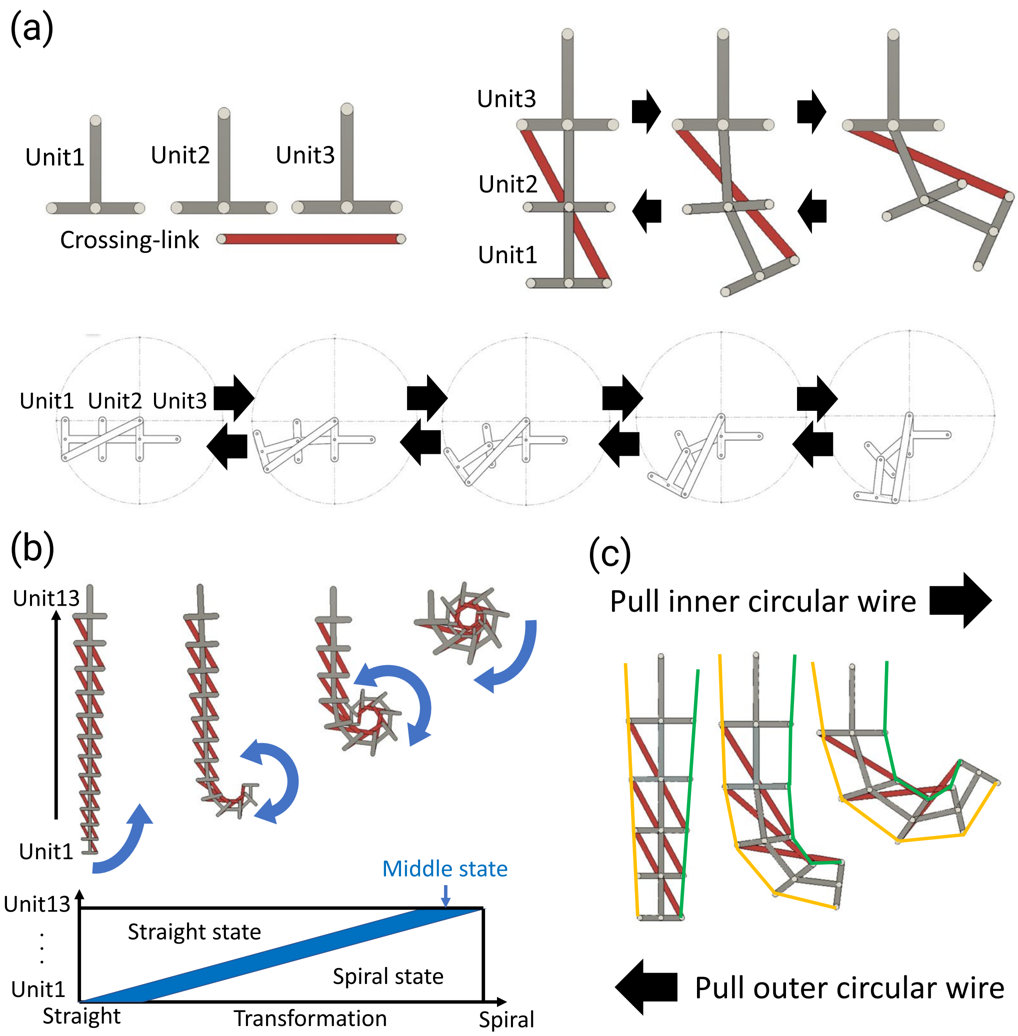

Fig. 1 Basic mechanism of the HSFM. **a** The minimum 4-bar link mechanism. **b** Transformation between straight and circular shapes. **c** Driving with wires

Mechanism

This section describes a base mechanism of the High-Strength and Flexible Mechanism (HSFM) and its 1st prototype.

Base mechanism

The basic structure of the HSFM comprises a series of four linkage mechanisms (Fig. 1a) [24]. The simplest mechanism consists of three T-shaped units and one crossing link: Fig. 1a. Unit 1 is connected to unit 2, unit 2 is connected to unit 3, and the crossing link is connected between one side of unit 1 and the opposite side of unit 3. Figure 1a show that the simplest mechanism's pose changes according to the crossing link's movements. Since the crossing link can rotate the opposite direction, a stopper to prevent the movement are necessary for actual usage. Although the mechanism is a simple closed-link mechanism, a mechanism that connects the units serially has three novel characteristics: mechanical constraints, wire drive, and smooth grounding function.

One of the novel characteristics is its mechanical constraints, which provide two features: high structural strength and flexible transformation. The constraints are justified by the number of the degree of freedom (DoF): DoF of the HSFM is always 1 even if the number of units constructing the HSFM is different. Based on Kutzbach-Gruebler's equation, the DoF of the simplest 4 link mechanism (Fig. 1a) is obtained as

$$DoF_3 = 3(L-1) - 2J = 3(4-1) - 2 \cdot 4 = 1 \quad (1)$$

where L and J are the numbers of links and pivot joints, respectively. When using five units (Fig. 1c), the DoF is also calculated as one:

$$DoF_5 = 3(L-1) - 2J = 3(8-1) - 2 \cdot 10 = 1 \quad (2)$$

Hence, the entire mechanism has one DoF. The detailed relationship between each unit is described in "Mechanical constraints" Section.

Due to the mechanical constraints, the HSFM performs a unique transformation between straight and spiral shapes, as shown in Fig. 1b. We define the units as unit 1 – unit n from the tip of the HSFM, as shown in Fig. 1b. Additionally, we defined the units posing a straight as a straight state, and those posing a spiral as a spiral state (Fig. 1b). The transformation starts from the tip, and the other units in the straight state do not move until the moving units approach the units. Hence, the straight state is not sensitive enough and can be regarded as a rigid body. The middle units are defined as a middle state in Fig. 1b, and the state shifts gradually according to the transformation. The units finishing the middle state become the spiral state. In the spiral state, the units reach a singular posture and can be regarded as a rigid body. These features are also seen in the reverse transformation from spiral to straight poses. Regarding structural strength, since some parts of the HSFM can be regarded as rigid bodies, its structure can be strong. We confirm that the HSFM can sufficiently support body weight without metallic material in "Strength for body weight support" Section.

Secondly, the HSFM is driven using wires (Fig. 1c). The wires are threaded through each unit and tied to the tip of the HSFM. When pulling up the wires tied to the inside of the spiral, the mechanism gradually changes toward a spiral pose and vice versa. This function enables us to transform and maintain the pose of the HSFM using wires, pulleys, and motors. The design of the driving system is explained in "1st prototype" Section. Additionally, the wire length is calculated in "Wire length" Section.

Finally, the HSFM rolls on the ground smoothly. The units in the spiral state rolls on the ground and changes its grounding point when transforming. This smooth grounding will help support body weight with shifts in a center of gravity of the user. We will show the demonstration of the grounding and trajectory measurement in "1st prototype" and "Grounding" Sections.

1st prototype

We developed the 1st prototype of the HSFM, as shown in Fig. 2. The 1st prototype was fabricated using a 3D

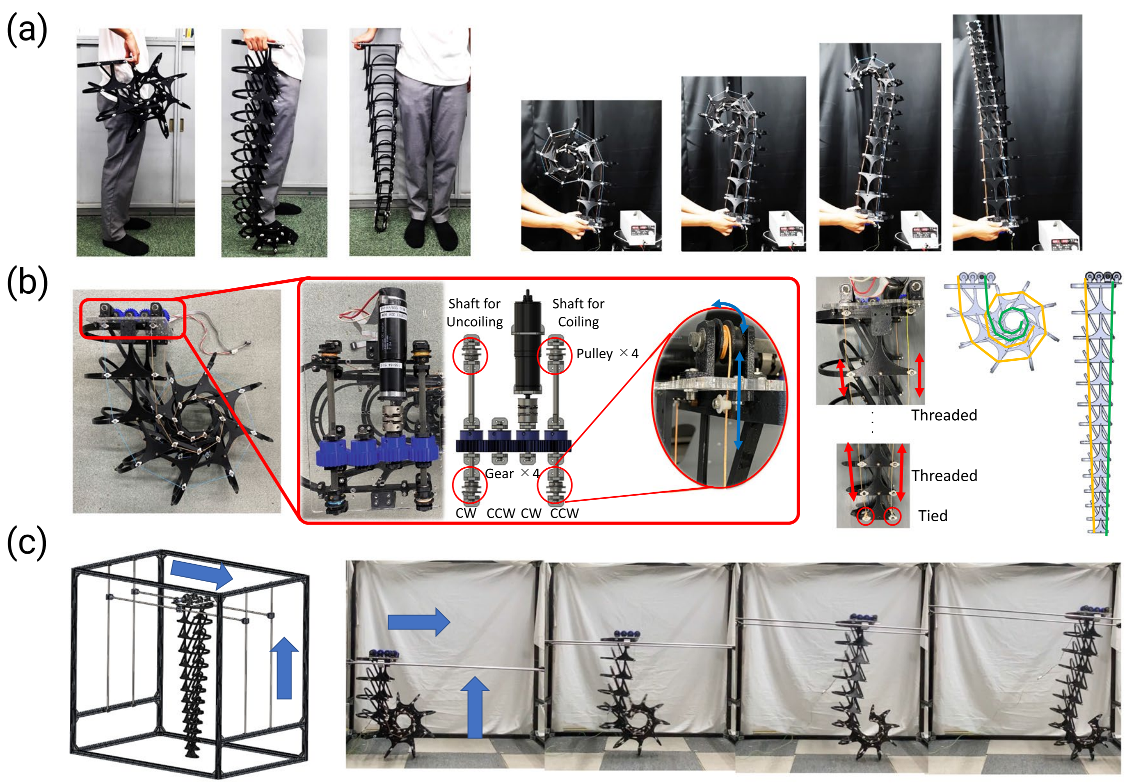

Fig. 2 The 1st prototype of the HSFM. **a** Flexible transformation between straight and spiral postures. **b** Wire-driven mechanism and wire paths. **c** Demonstration of the grounding function and its setup

printer Ultimaker3 and PLA (polylactic acid) material. The pivot joints were tightened with low-head bolts and nylon nuts. For a smooth rotation, a metal washier was inserted into every joint, and they got lubricated with grease. The whole mechanism comprised 13 units and was capable of housing its tip units inside its root units, as shown in Fig. 2a. The housing function was achieved by designing to increase unit size as it goes to the root. Its mass without the driving system is 0.8 kg, and the total mass is 2.0 kg. Detailed design policy was determined based on parametric analysis and will be explained in "Parametric analysis" Section. Additionally, its strength is evaluated with further design and fabrication in "Strength for body weight support" Section.

The wire-driven mechanism was constructed as shown in Fig. 2b. Four polyethylene wires were tightened to unit 1: two wires were for coiling and the others were for uncoiling. Every unit had four small holes that each wire goes through. The top of the mechanism had a driving system comprising one DC motor, four gears, four pulleys, and shafts. The motor rotates the pulleys and wounds the wires. The rotation direction of the pulleys was designed to be different: when the pulleys for uncoiling rotate clockwise, the pulleys for coiling rotate counterclockwise. This strategy leads to one advantage for the number of motors. In an easy design, when one motor wounds one wire, another motor needs to release another wire, which requires two motors and makes the control more complex. However, this driving system is designed to use one motor by wounding one wire and simultaneously releasing the other wire. The motor also can keep the tension force and the HSFM's posture with a position controller.

We demonstrated the grounding function of the mechanism: Fig. 2c. For the demonstration, a frame box was built with aluminum frames. The top of the 1st prototype was mounted on two poles. Since the mechanism cannot stand by itself, these poles played a role to support it. Linear bushes were attached to the poles and allow the 1st prototype to move in two directions. The units in the straight state of the 1st prototype was always kept vertical to the ground by the poles and linear bushes. Further, we drove the motor at a constant speed, and the mechanism moved as shown in Fig. 2c. The 1st prototype lifted the poles meanwhile shifting its grounding point. The 1st prototype did not break by the weight of the poles, which confirmed that the structural strength of the mechanism is high even with its plastic material.

Parametric analysis

This section conducts the parametric analysis and calculation on the HSFM's geometry.

Length ratio

The basic design of the HSFM was selected from seven parameter sets to obtain more strong mechanism (Fig. 3). The structural strength of the HSFM changes when the length ratio of the units changes. Stress analyses were conducted on Fusion 360 to evaluate their structural strength. A certain force was applied to the seven mechanisms in two postures: straight and circular. In the straight pose, a downward force is applied to the top of the mechanism, and the position of the bottom unit was locked. The results represent the strength of the straight state when supporting body weight. Regarding the circular pose, the tip of the mechanism experiences a force, and the top of the upper unit was locked. This force simulates the situation where a reaction force from environmental contact points is applied to the circular parts. In this comparison, the total height of the mechanisms was unified. In each set, the ratio between adjacent units is unified as 1.10. We assumed that the ratio should range from 1.05 to 1.15 to realize a spiral shape. 1.10 was selected as the average of the range.

First, the strength in the straight pose was higher in mechanisms (i), (iv), and (vii). Large displacements were not observed for any of the three mechanisms. The common property of these three mechanisms is that the length ratio between b and c is identical. The force could be distributed equally to the left (side of b) and right (side of c), which enhanced the strength of these mechanisms. When comparing mechanisms (ii) and (iii) in the straight pose, mechanism (iii) was influenced more by the vertical force. Similarly, mechanism (vi) was affected more than mechanism (v). These results clarify that a mechanism for which length c is longer than length b could be weaker than the mechanism for which c is shorter than b.

Second, mechanism (iv) is the strongest in the circular pose among the seven sets. We considered that the applied force could be distributed well in mechanism (iv): The crossing link is almost parallel to the bottom segment of each unit, which suppresses the increase in torque. Mechanisms (i), (ii), (v), and (vii) had similar characteristics regarding the angle, and their displacements were smaller than those of the other mechanisms. Mechanisms (iii) and (vi) in the circular pose were very weak against the reaction force from the ground.

Finally, based on these analyses, we adopt mechanism (iv), whose length ratio is a:b:c = 2:1:1.

Spiral shape

One of the advantages of this mechanism is its high expansion ratio. The advantage comes from the relative size of each unit. The size should be carefully determined because maximizing the extension ratio is

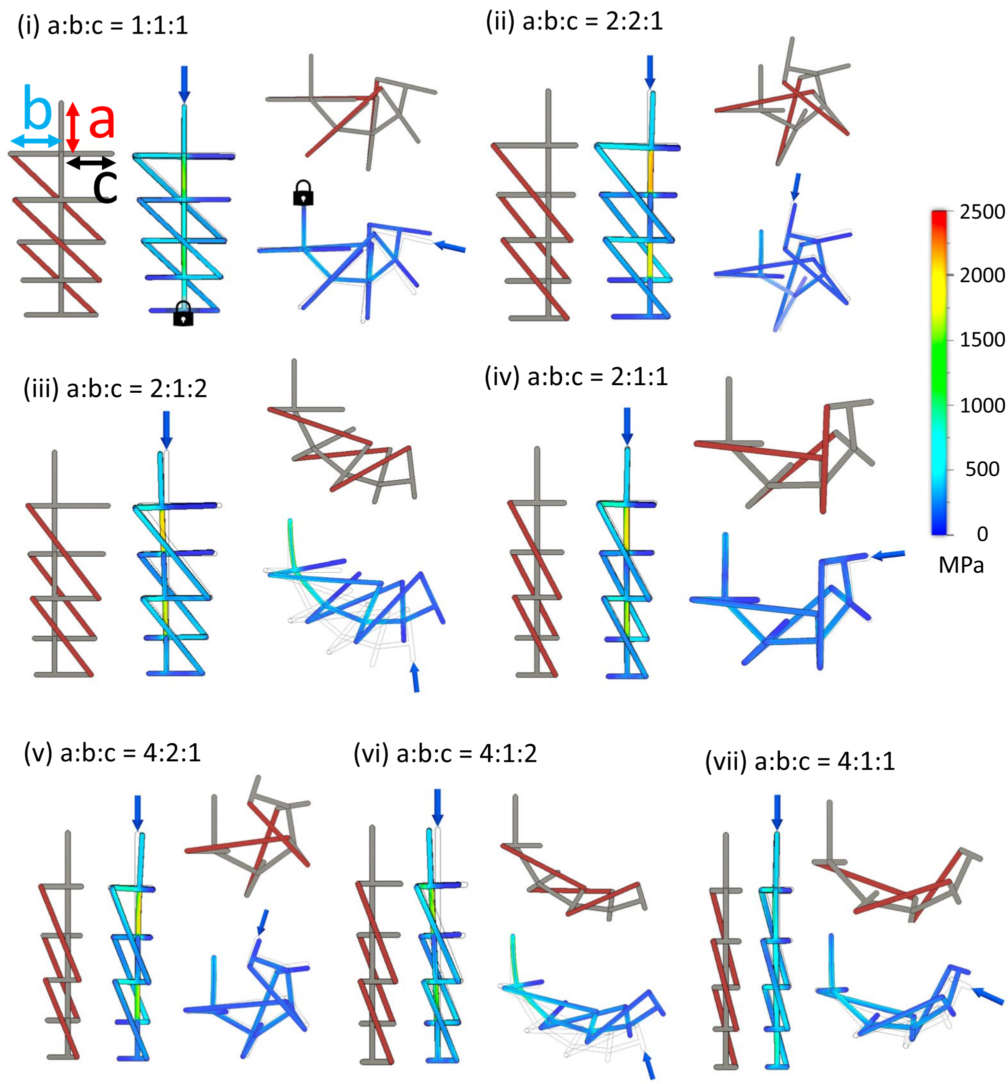

Fig. 3 Comparison of the strength of seven mechanisms with different length ratios. The blue arrow means the position and direction that the force is applied. The lock marker means that the position of the point is locked

required whilst avoiding conflicts between the parts is essential. The mechanism was designed based on spiral sketches. Spirals are ideal for this purpose because they can contain smaller circles inside the bigger one without any interference.

For the design, an Archimedes spiral is drawn, as shown in Fig. 4. Archimedes' spirals have equal space for each circle, which is useful for the design compared with other spirals such as logarithmic spirals and hyperbolic spirals. Next, the spirals are separated by 45 degrees each, and the length of each line is used as the unit's length a ("Length ratio" Section). 45 degrees was obtained from the 3D model in Fig. 3 (iv). Based on the length parameters, the HSFM was designed. As a result, a higher extension rate can be obtained.

Mechanical constraints

The length parameters were determined in "Length ratio" and "Spiral shape" Sections. Based on the parameters, the relationship between the units was calculated to clarify the mechanical constraints of the HSFM. Following mathematical formulas lead to the relationships. Figure 5a shows the parameters of the 4 linkage mechanism. To represent θ_2 as a function of θ_1, we solved the equation below:

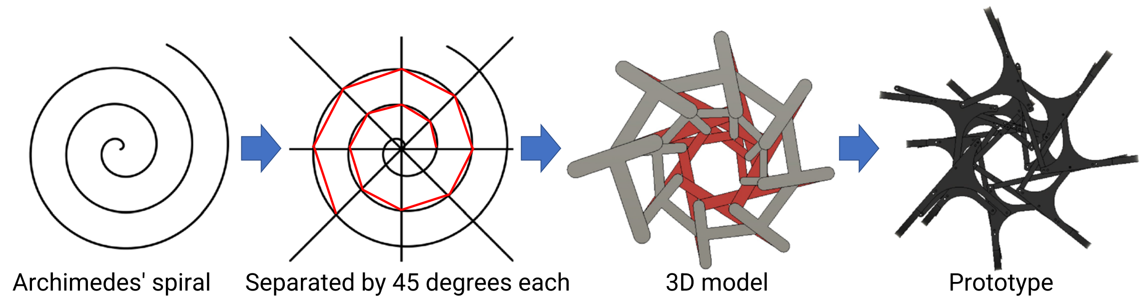

Fig. 4 Spiral sketch for designing the HSFM

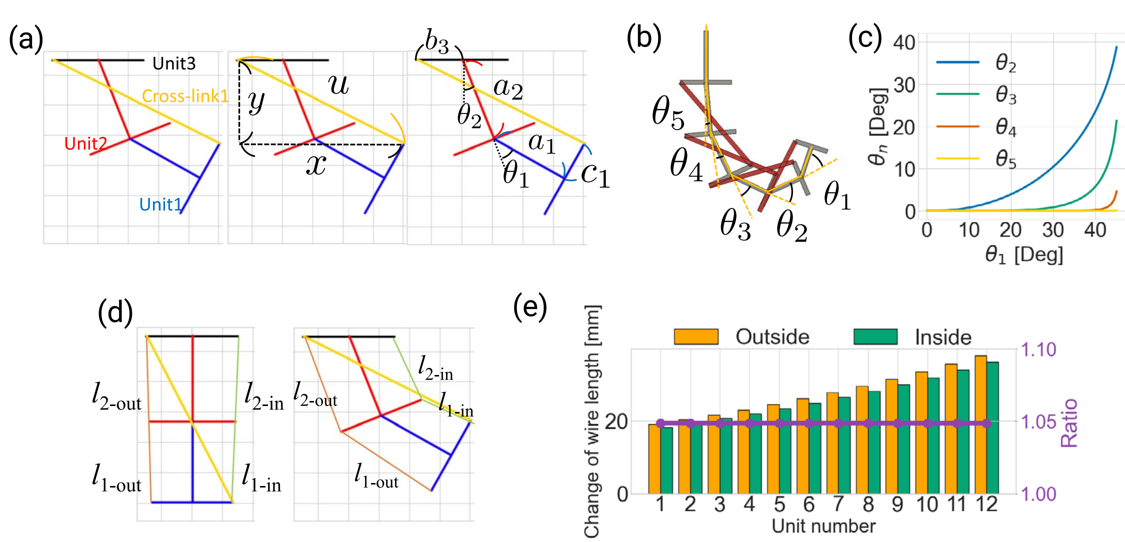

Fig. 5 The relationship between the posture of the units. **a** Symbols to represent the parameters of the 4 link mechanism for the mathematical formula. **b** Definition of angles θ. **c** Relationships between θ_1 and $\theta_2 - \theta_5$. **d** The definition of l_{out} and l_{in}. **e** Changes of wire length and ratio between *CWL* outside and inside in each unit

$$u^2 = x^2 + y^2 \tag{3}$$

Then, u, x, and y are represented as

$$u^2 = (c_1 + b_3)^2 + (a_1 + a_2)^2 \tag{4}$$

$$x = b_3 + a_2\sin\theta_2 + a_1\sin(\theta_1 + \theta_2) + c_1\cos(\theta_1 + \theta_2) \tag{5}$$

$$y = a_2\cos\theta_2 + a_1\cos(\theta_1 + \theta_2) - c_1\sin(\theta_1 + \theta_2) \tag{6}$$

where a, b, and c are defined in Fig. 5a. By substituting Eq. (4)–Eq. (6) to Eq. (3), θ_2 can be obtained as a function of θ_1.

$$\theta_2 = \sin^{-1}(\beta/\sqrt{\gamma^2 + \delta^2}) - \alpha \tag{7}$$

where α, β, γ and δ can be described as

$$\alpha = \tan^{-1}(\delta/\gamma) \tag{8}$$

$$\beta = c_1b_3 + a_2c_1\sin\theta_1 + a_1a_2(1 - \cos\theta_1) \tag{9}$$

$$\gamma = a_2b_3 + a_1b_3\cos\theta_1 - b_3c_1\sin\theta_1 \tag{10}$$

$$\delta = c_1b_3\cos\theta_1 + b_3a_1\sin\theta_1 \tag{11}$$

Based on this formula, the relative posture of each unit can be calculated. The relative angle between the units is defined as $\theta_1 - \theta_5$, as shown in Fig. 5b. Figure 5c shows that the angles $\theta_2 - \theta_5$ change according to the transition of θ_1. θ_2 is the most affected by the change in θ_1. In contrast, θ_5 was not influenced by the transition of θ_1 at all.

They do not have solutions when being over 45°, which means that the angles converge to a singular pose.

This relationship shows the mechanical constraints of the HSFM. The solution for each angle $\theta_2 - \theta_5$ for θ_1 was obtained uniquely, which means that the HSFM has only one DoF. θ_2 started to change when θ_1 exceeded 5°, and θ_2 was always smaller than θ_1. Similarly, θ_3 hardly moved until θ_2 began to change, and this tendency could be observed at every unit. Therefore, the transformation of the HSFM starts from its tip, and the root joint angle (θ_5) cannot be changed so much until a larger angular change occurs in the tip joint (θ_1). In detail, θ_5 keeps the straight state while θ_1 is in the middle state, and θ_5 becomes the middle state after θ_1 gets in the spiral state. These results confirmed that 4 contiguous units construct the middle state and the other units can be a rigid body. The mechanical constraints imply the structural strength of the HSFM. The actual strength is justified with the hardware in "Strength for body weight support" Section.

Wire length

In this section, we calculated the wire length. To control the HSFM's posture with one motor, the relationship between the amount of winding wire and the amount of releasing wire should be clarified. If the relationship is not carefully calculated, extra slack or tension will happen. When the ratio of the amount of both wires is constant, we can drive both simultaneously by designing the diameter of the pulleys that wind and release the wires.

The wire length is calculated with the same model that we used in "Mechanical constraints" Section. The wire's paths are made at the point of the edge of every unit (b and c in Fig. 3). We defined the length of wires outside and inside, $l_{n-\mathrm{out}}$ and $l_{n-\mathrm{in}}$, respectively (Fig. 5d). Then, n means the number of units. They are calculated in the following equations, respectively:

$$\begin{aligned} l_{n-\mathrm{out}}^2 &= (b_{n+1} + a_n \sin\theta_n - b_n \cos\theta_n)^2 \\ &\quad + (a_n \cos\theta_n + b_n \sin\theta_n)^2 \end{aligned} \tag{12}$$

$$\begin{aligned} l_{n-\mathrm{in}}^2 &= (-c_{n+1} + a_n \sin\theta_n - b_n \cos\theta_n)^2 \\ &\quad + (a_n \cos\theta_n - c_n \sin\theta_n)^2 \end{aligned} \tag{13}$$

where, a, b, c, and θ are defined in "Mechanical constraints" Section. The two wires change individual length simultaneously. The ratio of changes in the wire length must be the same for all n to avoid extra slack or tension of the wires. The changes in wire length can be defined as the difference between the length of the wire in the straight and spiral states. Since we have clarified that θ is 0 degrees in the straight state and 45 degrees in the spiral state, we substitute those values into the equations (12) and (13). Then, the changes of wire length outside and inside are defined as $CWL_{n-\mathrm{out}}$ and $CWL_{n-\mathrm{in}}$, respectively:

$$CWL_{n-\mathrm{out}} = l_{n-\mathrm{out}(\theta=45)} - l_{n-\mathrm{out}(\theta=0)} \tag{14}$$

$$CWL_{n-\mathrm{in}} = l_{n-\mathrm{in}(\theta=0)} - l_{n-\mathrm{in}(\theta=45)} \tag{15}$$

CWL of each unit is calculated and shown in Fig. 5e. $CWL_{n-\mathrm{out}}$ is always longer than $CWL_{n-\mathrm{in}}$. The ratio of CRL in each unit can be obtained as $Ratio_n$:

$$Ratio_n = CWL_{n-\mathrm{out}}/CWL_{n-\mathrm{in}} \tag{16}$$

Figure 5e shows $Ratio_n$ is always constant around 1.05. By designing the diameter of pulleys outside:inside = 1.05:1.00, two wires are driven simultaneously without extra slack or tension. Even if we changed the path of the wires, we can prevent extra slack or tension by changing the diameter of the pulleys.

Experiments and discussion

This section introduces the design of the 2nd prototype of the HSFM and evaluates its performance in terms of body weight support, and grounding function, and wire drive.

2nd prototype

The 2nd prototype was designed to have more strength, a higher grounding function, and a more compact size than the 1st prototype. Figure 6 shows the appearance of the 2nd prototype including interaction with a human, one-unit design, and size comparison. The mass of the 2nd prototype was designed 2.0 kg. It can transform between spiral and straight poses in 1 s.

First, to enhance its strength, carbon fiber printing technology (Markforged Mark Two) was used. The parts were printed with two nozzles, extruding onyx and carbon fiber. The outside of the parts is covered by Onyx, and the inside is filled with the carbon fiber. The printed material's strength is stated to be equivalent to that of aluminum 6061-T6 [25]. Detailed analysis of stiffness will be provided in "Strength for body weight support" Section.

Second, the grounding function was improved: The shape of the grounding area was designed to be an arc, as shown in Fig. 6b. The arc was depicted as a circle passing through the grounding points of three successive units. Moreover, it was designed to avoid conflicts between successive units. The strength of the arc shape is analyzed in "Strength for body weight support" Section, and the evaluation of the grounding function is demonstrated in "Grounding" Section.

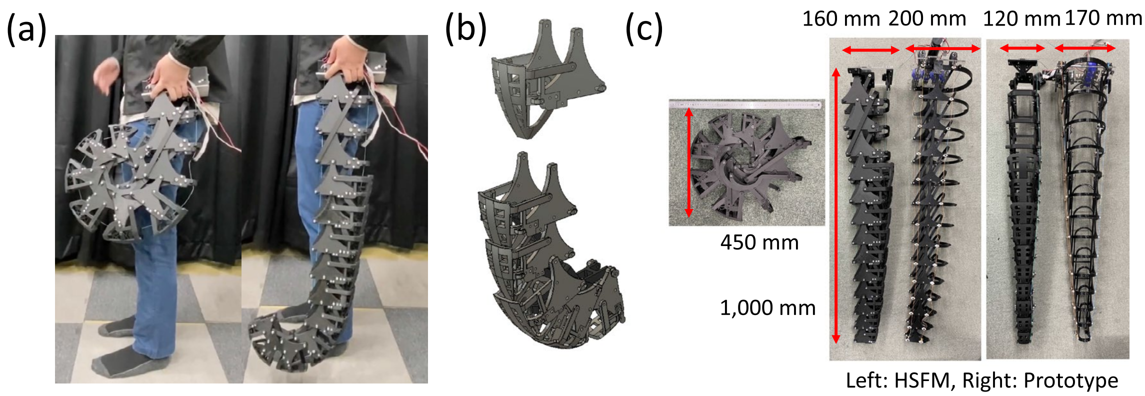

Fig. 6 High-Strength and Flexible Mechanism. **a** Interaction with a human. **b** One unit design and five consecutive units. **c** Size comparison with the prototype

Finally, the size became more compact than the 1st prototype: Fig. 6c. Although the 1st prototype changes the unit's width gradually, the 2nd prototype unified the width of the tip and root units, respectively. Additionally, the arc shape of the root units was not designed because they do not touch the ground, which contributed to the downsizing. The length in the straight posture is 1000 mm and that in the spiral posture is 450 mm. In this paper, the extension rate is defined as the rate of maximum length to minimum length. We achieved 2.22 extension rate, which is very high compared with simple linear actuators.

Strength for body weight support

The strength of the HSFM was evaluated through both simulation and real-world experiments. In the simulation, the strength of the arc shape was analyzed. We assumed that a large force (30 kg) was applied to the tip of the arc shape and its material was aluminum. Figure 7a shows the arc parts are hardly deformed. The minimum safety factor of the parts was more than 5, showing enough strength.

Simultaneously, the strength of the crossing links has a big impact on the structural strength. Since these links are long, they are more susceptible to forces and moments than T-shape units. In particular, buckling should be taken care of. The buckling behavior in structural mechanics can be represented as Euler's buckling equation. It relates the critical buckling load to the properties of the structure. The equation is as follows:

$$F = \frac{C\pi^2 EI}{L^2} \tag{17}$$

where F is the critical buckling load, which represents the minimum load required to cause buckling. E, I, and L is the modulus of elasticity of the material, the second moment of area, and effective length of the structure.

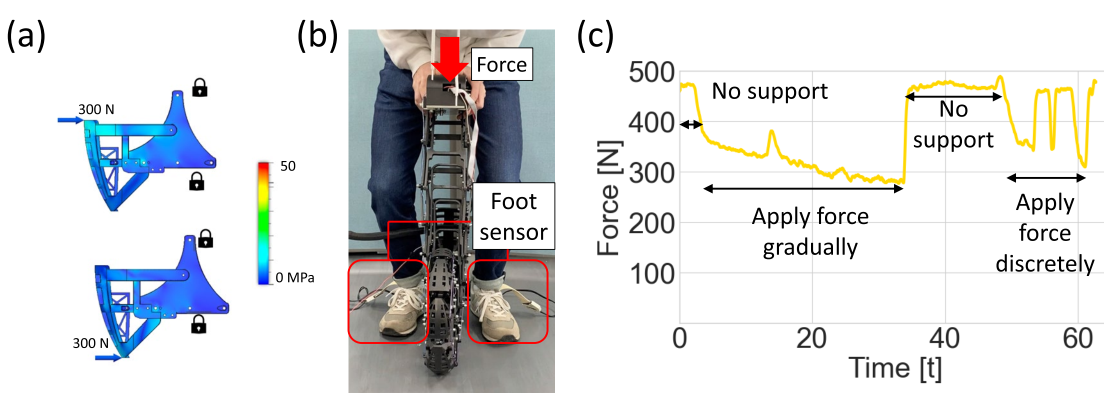

Fig. 7 Strength was analyzed through simulation and real-world experiments. **a** Simulation of the strength of the arc shape. Blue arrow means force (300 N) applied to the parts. Lock marker means that the positions of the point (2 holes) are locked. **b** Setup of the real-world experiments. **c** Time-series data of the reaction force from the ground to the feet (total of both feet)

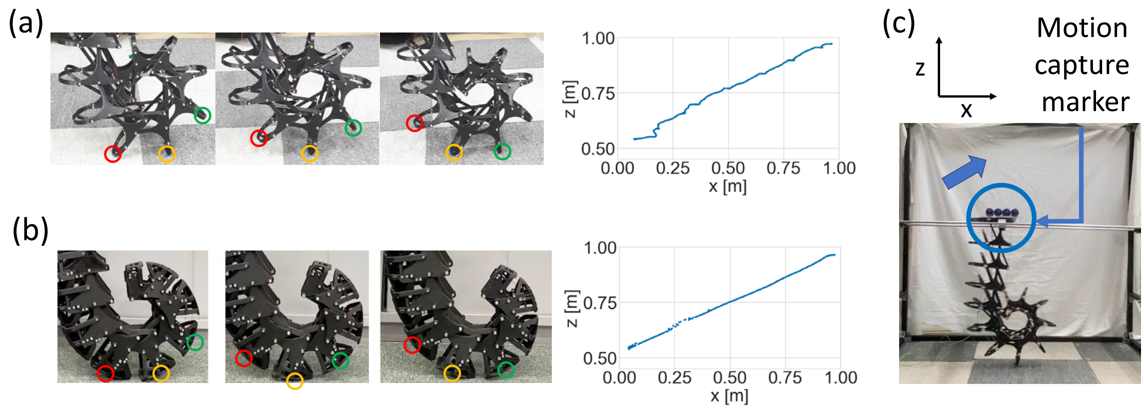

Fig. 8 Experiments demonstrating the grounding function. **a** The grounding images and the trajectory of the 1st prototype's top. The colored circles express certain grounding points. **b** Those of the 2nd prototype. **c** Condition of the measurement

C is the constant value whose value depends on the conditions of end support of the column. To enhance the strength against buckling, we increase the second moment of area I. The cross-section of this link is rectangular, and its second moment of area I is expressed by the following equation with its width b and height h.

$$I = \frac{bh^3}{12} \tag{18}$$

The greater I gets, the less likely the part is to bend. Hence, h should be designed to be long to get high strength.

In real-world experiments, the 2nd prototype's strength was confirmed through human interaction. We measured how much weight the 2nd prototype can support when a person leaned over it. The subject wore a foot plantar pressure measurement system (Pedar) [26, 27]. The sampling frequency was 50 Hz, and the signals were smoothed with a moving average method at 0.1 s windows. The mechanism's posture was locked with a position control of the motor and wires.

Figure 7b shows the setup of the experiment and (c) shows the time-series data of the foot force (total of both feet). The initial foot force was the subject's body weight in the case without the support and was 470 N. The subject gradually leaned his weight on the 2nd prototype, which reduced the foot force to 280 N. In addition, the weight was applied suddenly with impact force from 50 s to 60 s. The forces did not cause a major transformation of the mechanism nor damage to the driving system. Applying larger force was prevented due to a human's balancing ability. The results confirmed that the 2nd prototype can support 200 N weight. Further, we plan to use a couple of HSFMs in the development of assistive robots in the future. They will support more than 400 N or 600 N body weight, which can be enough to support the whole body of the user.

There is an offset between the ground point and the position of the top of the HSFM, which can affect the performance of body weight support. This offset can generate a moment when the HSFM supports body weight. Since the moment may act on breaking the HSFM and making the HSFM slip on the ground, further experiments will be conducted in the future.

Grounding

The grounding function of the first and 2nd prototypes were analyzed. Figure 8's colored circles show that the grounding parts of the prototype were discrete and shifts of the grounding point were rough. In contrast, the 2nd prototype was designed to make the shifts smooth: The grounding area has circular parts and the shifts are continuous. The prototypes were driven using the wires and the DC motor at a constant speed. The trajectories of the top of them were measured using an optical motion capture system (Opti Track). Figure 8 shows the trajectory of the prototypes. The top parts went up from 500 mm height to 1000 mm height while shifting 1000 mm on the ground. The 1st prototype's trajectory had an uneven line. In contrast, the 2nd prototype demonstrated a smooth line: The effectiveness of the circular arc parts

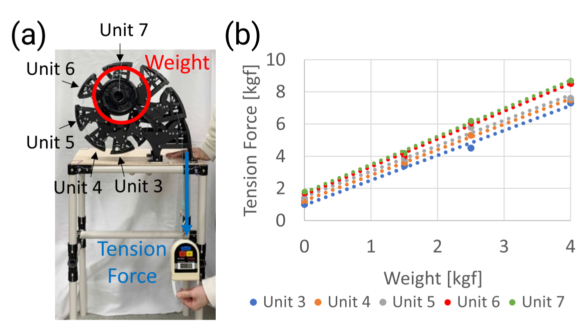

Fig. 9 Experiments to investigate the required tension force. **a** Setup of the experiment. **b** Relationship between the tension force and the weight that the 2nd prototype supports

Table 1 The parameters represent the relationship of the tension force and the weight

Unit	3	4	5	6	7	Average
Slope	1.54	1.58	1.57	1.72	1.74	1.63
Intercept	0.95	1.23	1.49	1.62	1.74	1.41

was confirmed. This function will contribute to the comfortableness of the assistance.

Wire driven

Static force experiments were conducted to estimate the tension force required of wire to support body weight. The experimental setup is shown in Fig. 9a. The 2nd prototype was placed on a desk and the weight was hung from the top of it using a string. Weights of 0, 1.5, 2.5, and 4 kg were used. A digital spring scale was tied to the tip of the wire and was pulled until the prototype starts to move. Since the results may differ from the HSFM's posture, the measurements were conducted in several postures. Figure 9a shows that unit 7 was set in the highest position and hung the weight. Following that, the other units (3–6) were also set at the top and the weight was applied.

Figure 9b shows the results of this experiment. The points represent the required tension force in each condition: four types of weights and five units to which the weight was hung. The dotted lines were obtained using the least-squares method. The parameters of the lines are represented as

$$(Tension) = (Slope) \times (Weight) + (Intercept) \quad (19)$$

where Table 1 shows *Slope* and *Intercept*. No significant differences were observed between the slope of the lines (mean gradient = 1.63). However, the initial tension force (*Intercept* in Table 1) increased as the number of units increased. We considered that the weight of the mechanism itself had a slight impact on the increase of *Intercept*. However, the gaps of *Intercept* can be ignored when values of weight are large such as body weight. Assuming that the 2nd prototype supports 20 kg, 320 N will be required as the tension force (Additional file 1).

Conclusion

In conclusion, this paper proposed the High-Strength and Flexible Mechanism (HSFM) for limb-type assistive robots. The HSFM can transform between straight and spiral poses while maintaining high strength due to its mechanical constraints. The constraints were analyzed based on the geometric calculation. Due to the design based on Archimedes' spiral, a 2.2 extension rate was obtained. In addition, the HSFM's driving methodology was achieved with just one motor and wires, contributing to a simple control system. Furthermore, the experiments confirmed that the HSFM can support 20 kg and shift its grounding point smoothly. The required tension force of the wires was also investigated for future applications.

One limitation of this paper is the HSFM's size. We plan to use HSFM in a straight state for the assistance of walking. Although it achieved a high extension rate, it may disturb the wearer doing daily living activities. We will focus on downsizing the HSFM in the future. Since its size depends on the diameter of the spiral, the further design will start from the sketch of the spiral again. In addition, we will improve designs that could cause entrapment of fingers or clothing. Furthermore, the HSFM's performance in practical scenarios such as sit-to-stand and walking should be evaluated. For the application, appropriate control systems and wearable segments will be developed in the future.

Supplementary Information

The online version contains supplementary material available at https://doi.org/10.1186/s40648-023-00255-x.

Additional file 1: Supplement.mp4. This video shows the unique movement of the HSFM.

Acknowledgements
Not applicable.

Author contributions
SS developed the mechanism, carried out all experiments, analyzed data and wrote the paper. UJ developed the 1st prototype of the mechanism. YZ gave advises on analysis of data and paper writing. YH initiated this project and gave advises on the design and paper writing. All authors read and approved the final manuscript.

Funding
This work is supported by JST [Moonshot R &D], [Grant Number JPMJMS2034].

Availability of data and materials
The data supporting the findings of this study are available from the corresponding author, SS, upon reasonable request.

Declaration

Competing interests
The authors declare that they have no competing interests.

Received: 18 April 2023 Accepted: 17 June 2023
Published online: 15 July 2023

References

1. Huang J, Yan S, Yang D, Wu D, Wang L, Yang Z, Mohammed S (2021) Proxy-based control of intelligent assistive walker for intentional sit-to-stand transfer. IEEE/ASME Transactions on Mechatronics 27(2):904–915
2. Mou W-H, Chang M-F, Liao C-K, Hsu Y-H, Tseng S-H, Fu L-C (2012) Context-aware assisted interactive robotic walker for parkinson's disease patients. In: 2012 IEEE/RSJ International Conference on Intelligent Robots and Systems, pp. 329-334. IEEE
3. Kataoka N, Hirai H, Hamilton T, Yoshikawa F, Kuroiwa A, Nagakawa Y, Watanabe E, Ninomaru Y, Saeki Y, Uemura M, *et al.* (2017) Effects of partial body-weight support and functional electrical stimulation on gait characteristics during treadmill locomotion: Pros and cons of saddle-seat-type body-weight support. In: 2017 International Conference on Rehabilitation Robotics (ICORR), pp. 381–386 . IEEE
4. OpeMed: Walking Harness (Loops). https://www.opemed.net/product/walking-harness-loops/
5. Wang S, Wang L, Meijneke C, Van Asseldonk E, Hoellinger T, Cheron G, Ivanenko Y, La Scaleia V, Sylos-Labini F, Molinari M et al (2014) Design and control of the mindwalker exoskeleton. IEEE Transa Neural Syst Rehabilitation Eng 23(2):277–286
6. Lee S, Karavas N, Quinlivan BT, LouiseRyan D, Perry D, Eckert-Erdheim A, Murphy P, Goldy TG, Menard N, Athanassiu M *et al.*: (2018) Autonomous multi-joint soft exosuit for assistance with walking overground. In: 2018 IEEE International Conference on Robotics and Automation (ICRA), pp. 2812–2819 . IEEE
7. Tsukahara A, Kawanishi R, Hasegawa Y, Sankai Y (2010) Sit-to-stand and stand-to-sit transfer support for complete paraplegic patients with robot suit hal. Advanced Robotics 24(11):1615–1638
8. Kulasekera AL, Arumathanthri RB, Chathuranga DS, Gopura R, Lalitharatne TD (2021) A low-profile vacuum actuator (lpvac) with integrated inductive displacement sensing for a novel sit-to-stand assist exosuit. IEEE Access 9:117067–117079
9. Parietti F, Asada H (2016) Supernumerary robotic limbs for human body support. IEEE Trans Robot 32(2):301–311
10. Davenport C, Parietti F, Asada HH (2012) Design and biomechanical analysis of supernumerary robotic limbs. In dynamic systems and control conference. Am Soc Mech Eng 45295:787–793
11. Treers L, Lo R, Cheung M, Guy A, Guggenheim J, Parietti F, Asada H (2016) Design and control of lightweight supernumerary robotic limbs for sitting/standing assistance. In: International Symposium on Experimental Robotics. Springer, Berlin
12. Wu X, Liu H, Liu Z, Chen M, Wan F, Fu C, Asada H, Wang Z, Song C (2020) Robotic cane as a soft superlimb for elderly sit-to-stand assistance. In: 2020 3rd IEEE International Conference on Soft Robotics (RoboSoft), pp. 599–606. IEEE
13. Buckingham R (2002) Snake arm robots. Industrial Robot Int J 29(3):242–245
14. Marchese AD, Komorowski K, Onal CD, Rus D (2014) Design and control of a soft and continuously deformable 2d robotic manipulation system. In: 2014 IEEE International Conference on Robotics and Automation (ICRA), pp. 2189–2196 . IEEE
15. Tadakuma K, Fujimoto T, Watanabe M, Shimizu T, Takane E, Konyo M, Tadokoro S (2020) Fire-resistant deformable soft gripper based on wire jamming mechanism. In: 2020 3rd IEEE International Conference on Soft Robotics (RoboSoft), pp. 740–747. IEEE
16. Matsuo H, Asada HH, Takeda Y (2020) Design of a novel mutliple-dof extendable arm with rigid components inspired by a deployable origami structure. IEEE Robot Autom Lett 5(2):2730–2737
17. Shah SIH, Bashir S, Ashfaq M, Altaf A, Rmili H (2021) Lightweight and low-cost deployable origami antennas-a review. IEEE Access 9:86429–86448
18. Natsume R, Hoshiba K, Sugahara Y, Takeda Y, Shimono S (2022) Design of origami-inspired fall prevention device based on portability and extension characteristics. Proceedings of the 5th Jc-IFToMM International Symposium
19. El-Khasawneh BS, Ferreira PM (1999) Computation of stiffness and stiffness bounds for parallel link manipulators. Int J Mach Tools Manuf 39(2):321–342
20. Dagalakis NG, Albus JS, Wang B-L, Unger J, Lee JD (1989) Stiffness study of a parallel link robot crane for shipbuilding applications
21. Maden F, Korkmaz K, Akgün Y (2011) A review of planar scissor structural mechanisms: geometric principles and design methods. Archit Sci Rev 54(3):246–257
22. Akgün Y, Gantes CJ, Kalochairetis KE, Kiper G (2010) A novel concept of convertible roofs with high transformability consisting of planar scissor-hinge structures. Eng Struct 32(9):2873–2883
23. Hahm KS, Asada HH (2019) Design of a fail-safe wearable robot with novel extendable arms for ergonomic accommodation during floor work. In: 2019 IEEE/RSJ International Conference on Intelligent Robots and Systems (IROS), pp. 8179–8184 . IEEE
24. Liu X, Wang C, McCarthy JM (2020) The design of coiling and uncoiling trusses using planar linkage modules. Mechanism Mach Theory 151:103943
25. Markforged: Carbon Fiber The backbone of aluminum-strength composite parts. https://markforged.com/materials/continuous-fibers/continuous-carbon-fiber
26. Abdul Razak AH, Zayegh A, Begg RK, Wahab Y (2012) Foot plantar pressure measurement system: a review. Sensors 12(7):9884–9912
27. Novel-Quality-in-Measurement: Pedar. https://www.novel.de

Publisher's Note